Research article

# Novel prognostic model of complement and coagulation cascade-related genes correlates with immune environment and drug sensitivity in hepatocellular carcinoma

Hui Su [a,b,c], Yunjie Chen [a], Wuke Wang [a,*]

[a] *Department of General Surgery, Ningbo No. 2 Hospital, Ningbo, Zhejiang, China*
[b] *Ningbo Institute of Life and Health Industry, Ningbo No.2 Hospital, Ningbo, Zhejiang, China*
[c] *Key Laboratory of Diagnosis and Treatment of Digestive System Tumors of Zhejiang Province, Ningbo, Zhejiang, China*

## ARTICLE INFO

## ABSTRACT

*Introduction:* Hepatocellular carcinoma (HCC) is an immunogenic cancer characterized by high morbidity and mortality rates. The complement and coagulation systems are traditionally associated with the incidence of thrombotic complications and complement activation in cancer. However, the prognostic value of complement and coagulation-related factors (CCCR) in HCC remains undetermined. This study aims to construct a prognostic model based on the complement and coagulation cascades to evaluate its potential for immunotherapy and its relationship with drug sensitivity.

*Materials and methods:* We comprehensively investigated the expression profiles of CCCR genes using the TCGA, ICGC, and GTEx databases. Cox proportional hazards regression models were employed to assess prognostic value.

*Results:* This study presents a novel prognostic model derived from the comprehensive analysis of nine CCCR genes (C1S, C6, C7, F11, F13B, F7, SERPINE1, SERPINF2, and SERPING1) to elucidate their correlation with the tumor immune environment and drug sensitivity in patients with HCC. Our model stratified patients into high- and low-risk groups based on distinct survival outcomes. The area under the curve (AUC) values of the risk score for one-, two-, and three-year survival rates were all greater than 0.660. Additionally, we analyzed immune cell infiltration patterns, revealing a strong correlation between CCCR gene expression and the immune microenvironment, including T cell and macrophage activity. Our findings also identified potential therapeutic targets, demonstrating differential drug sensitivity profiles between the risk groups. JAK1_8709_1718 was found to be more suitable for patients with low-risk HCC.

*Conclusion:* Our findings provide promising insights into the clinical relevance of CCCR genes as prognostic markers and therapeutic targets. This study underscores the significance of CCCR in HCC and paves the way for improved therapeutic strategies.

## 1. Introduction

Hepatocellular carcinoma (HCC), the most prevalent type of liver cancer worldwide, has become the third leading cause of cancer-

---

* Corresponding author.
*E-mail address:* a88960317@163.com (W. Wang).

related deaths due to its high morbidity and mortality rates [1]. Despite the approval of various treatments, including surgical resection, chemoradiotherapy, and targeted pharmacological therapy, HCC still constitutes 75%–85 % of primary liver cancers and is associated with a poor prognosis [2]. Tumors often spread before diagnosis because of the lack of early symptoms in many patients. Additionally, traditional clinical parameters such as alpha-fetoprotein (AFP) and TNM staging are limited in their prognostic utility due to the complex molecular mechanisms and high heterogeneity of liver cancer [3]. Therefore, there is an urgent need for more accurate prognostic models to predict outcomes and guide effective treatment.

Recently, immunotherapies have emerged as important tools in cancer treatment, demonstrating impressive progress [4]. Consequently, advancements in immunotherapy have highlighted the importance of the immune microenvironment in improving the prognosis of patients with HCC. The complement and coagulation systems, traditionally known as liver-derived components of immunity, are associated with the incidence of thrombotic complications and complement activation in cancer [5]. Notably, several studies have reported that differentially expressed genes related to the complement and coagulation pathways are enriched in HCC [6–8]. Zhang et al. identified that the gene C8B, downregulated in the complement and coagulation cascade signaling pathways, can serve as a prognostic biomarker for survival in patients with HBV-related HCC [9]. However, proteomic analyses have shown increased levels of complement cascade-related proteins in HCC [10]. In light of these contradictory findings, we propose that the complement and coagulation cascades are related to cancer prognosis.

In this study, complement and coagulation cascade-related (CCCR) genes were established and validated. We subsequently evaluated the clinical prognosis, immune microenvironment, and drug sensitivity of patients with HCC. This research provides an exciting opportunity to advance our understanding of prognostic prediction and develop promising new therapeutic approaches for HCC.

## 2. Materials and methods

### 2.1. Data acquisition

The analytical process used in this study is shown in Fig. S1. The mRNA expression dataset was obtained from the University of California Santa Cruz Xena browser (http://xena.ucsc.edu) and the International Cancer Genomics Consortium (ICGC). Samples lacking survival status and time were filtered out, retaining expression profiles and clinical information. To ensure dataset comparability and minimize batch effects, a uniform normalization procedure was applied across all datasets. Specifically, since GTEx data were logged as log2(fpkm+0.001) and TCGA data as log2(fpkm+1), both were converted to FPKM values for differential analysis using the limma package. Batch effects were mitigated using the normalize BetweenArrays function in the limma package [11]. The UCSC Xena database served as the training cohort, comprising 371 HCC tumor samples and 276 normal samples (50 from TCGA and 226 from GTEx). The ICGC database served as the validation cohort, including 231 HCC samples. Detailed patient information from the training and validation cohorts is presented in Table 1.

### 2.2. Analysis of CCCR genes

Gene expression was normalized to fragments per kilobase of transcript per million (FPKM) for subsequent analyses. CCCR genes were sourced from the Kyoto Encyclopedia of Genes and Genomes (KEGG) database to construct a risk score for predicting HCC prognosis. The Wilcoxon test identified differentially expressed genes (DEGs) between tumor and normal groups (adjusted P-value

**Table 1**
Clinical characteristics of patients with HCC in training and testing datasets.

| Covariates | Type | Total, n (%) | Group, n (%) | |
|---|---|---|---|---|
| | | | Testing | Training |
| Age | | | | |
| | ≤65 | 321 (53.32) | 89 (38.53) | 232 (62.53) |
| | >65 | 280 (46.51) | 142 (61.47) | 138 (37.2) |
| | Unknown | 1 (0.17) | 0 (0) | 1 (0.27) |
| Sex | | | | |
| | Female | 182 (30.23) | 61 (26.41) | 121 (32.61) |
| | Male | 420 (69.77) | 170 (73.59) | 250 (67.39) |
| Grade | | | | |
| | G1 | 91 (15.12) | 36 (15.58) | 55 (14.82) |
| | G2 | 282 (46.84) | 105 (45.45) | 177 (47.71) |
| | G3 | 193 (32.06) | 71 (30.74) | 122 (32.88) |
| | G4 | 31 (5.15) | 19 (8.23) | 12 (3.23) |
| | Unknown | 5 (0.83) | 0 (0) | 5 (1.35) |
| Stage | | | | |
| | Stage I | 202 (33.55) | 31 (13.42) | 171 (46.09) |
| | Stage II | 245 (40.70) | 159 (68.83) | 86 (23.18) |
| | Stage III | 106 (17.61) | 21 (9.09) | 85 (22.91) |
| | Stage IV | 6 (1.00) | 1 (0.43) | 5 (1.35) |
| | Unknown | 43 (7.14) | 19 (8.23) | 24 (6.47) |

<0.05). Upregulated genes were defined as a fold change (FC) greater than 1.5 and downregulated genes were defined as a FC less than −1.5. Significant DEGs underwent univariate Cox regression analysis to identify prognosis-related genes (PRGs) (adjusted P-value <0.05). The R package "Veen" was employed to extract overlapping DEGs and PRGs. Correlation analysis of prognosis-related CCCR genes utilized the corrplot and ggplot2 R packages.

### 2.3. Development and assessment of prognostic risk model

To assess the prognostic value of CCCR genes, overlapping DEGs and PRGs underwent LASSO Cox regression [11–13]. Regression coefficients were calculated to establish a prognostic risk score formula based on gene expression levels. Subsequently, training and validation groups were stratified into high- and low-risk categories using the median risk score as a cutoff. Survival analysis was conducted and graphically represented for both groups using R packages "Survival" and "survminer." Univariate and multivariate Cox regression analyses were performed to evaluate the prognostic independence of risk scores in conjunction with clinical features, visualized via forest plots incorporating sex, age, TNM stage, grade, and risk score. The predictive accuracy of the model for 1-year, 2-year, and 3-year overall survival was assessed using receiver operating characteristic (ROC) curves and the consistency index (C-index). A nomogram was constructed to predict survival probability based on the risk score and clinical factors. Principal component analysis (PCA) and t-distributed Stochastic Neighbor Embedding (tSNE) were employed for dimensionality reduction to visually illustrate the ability of the model to differentiate samples in the low- and high-risk groups.

### 2.4. Functional and pathway enrichment analysis

DEGs between low- and high-risk groups in the entire cohort were analyzed using the Wilcoxon test (adjusted P-value <0.05 and |
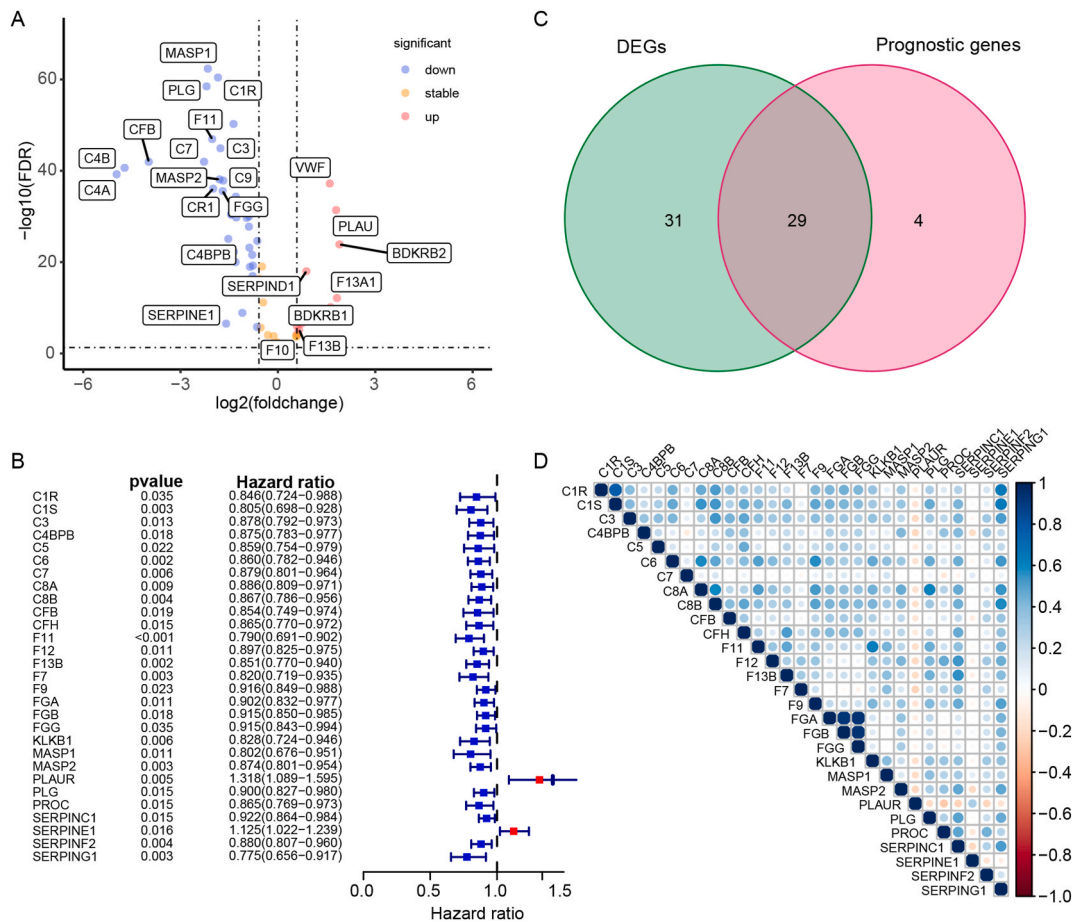


**Fig. 1.** Identification of DEGs related to complement and coagulation cascades in the training cohort between HCC tumor samples (N = 371) and normal samples (N = 276). (A) Volcano plot showing differential expression of CCCR genes between tumor tissues and adjacent normal tissues. (B) Forest plot displaying hazard ratios (HRs) and 95 % confidence intervals (CIs) for 29 prognostic CCCR genes in HCC. The vertical dashed line at HR = 1 indicates the threshold where genes are considered neither protective nor risk factors. HR > 1 was protective gene and HR < 1 was risk gene. (C) Venn diagram of differential and prognostic genes. (D) Heatmap depicting correlations among 29 prognostic CCCR genes.

log2 fold change (FC)| ≥ 0.58). GO and KEGG pathway enrichment analyses were conducted to elucidate the functional roles and signaling pathways of these DEGs.

## 2.5. Immune cell infiltration

Quantification of tumor-infiltrating immune cells and immune function differences between low- and high-risk groups was performed using single-sample gene set enrichment analysis (ssGSEA) and the CIBERSORT algorithm [14,15]. Box plots illustrated the variations in immune cell infiltration between the groups. Furthermore, Spearman's test evaluated the relationship between the risk score and infiltrating immune cells. Validation of tumor-infiltrating immune cells and immune function utilized GSE14520 and GSE16757 datasets from the Gene Expression Omnibus (GEO) database (https://www.ncbi.nlm.nih.gov/geo/).

## 2.6. Chemotherapeutic drugs response with prognostic risk model for patients with HCC

The tumor immune dysfunction and exclusion (TIDE, http://tide.dfci.harvard.edu/) algorithm, which considers tumor intrinsic factors and host immune responses critical for immunotherapy outcomes [16], integrated gene expression data with predefined gene signatures reflecting aspects of immune responses (e.g., T cell exhaustion, dysfunction, exclusion).

To assess the prognostic utility of the risk score model in guiding HCC treatment decisions, we employed the R package "Onco-Predict." This involved analyzing the susceptibility of HCC cells to chemotherapeutic drugs using expression matrix and half-maximal inhibitory concentration (IC50) data from the Genomics of Drug Sensitivity in Cancer (GDSC) database (https://www.cancerrxgene.org/). The "calcPhenotype" function was utilized to derive drug response phenotypes for each sample in training and validation cohorts. Boxplots visualized and compared sensitivity to various targeted drugs between high- and low-risk groups.

## 2.7. Statistical analysis

All statistical analyses were conducted using RStudio (v.4.2.0) and relevant packages, as detailed previously. Statistical significance for general clinical characteristics analyzed using SPSS software was set at two-tailed, with $P < 0.05$. Continuous variables are presented as mean ± standard deviation and were assessed using Student's $t$-test or Wilcoxon test. Categorical variables are expressed as frequencies and proportions and analyzed using the chi-square and Fisher's exact tests.

## 3. Result

### 3.1. Expression and prognostic values of CCCR genes in training patients with HCC

Sixty-nine CCCR genes were sourced from the KEGG (KEGG_COMPLEMENT_AND_COAGULATION_CASCADES.v2023.1. Hs.gmt). In the training cohort, 47 DEGs were identified, comprising 20 down-regulated and 27 up-regulated CCCR genes. As depicted in Fig. 1A, notable DEGs included MASP1, PLG, C1R, F11, CFB, C7, C3, C4A, C4B, MASP, C9, and others, while PLAU, BDKRB1, BDKRB2, F13A1, SERPIND1, and F13B were upregulated. To assess the prognostic significance of CCCR genes, univariate Cox regression analysis was employed to select significant PRGs (Fig. 1B). Integration of differentially and prognostically significant genes identified 29 CCCR genes, predominantly characterized as risk factors (Fig. 1C). Utilizing a correlation heatmap, it was observed that most prognostic CCCR genes exhibited negative correlations among themselves, except for PLAUR (Fig. 1D).

### 3.2. Development and validation of risk model based on CCCR genes

LASSO Cox regression analysis was utilized to identify independent prognostic factors among CCCR genes (Fig. 2A and **B**). Using weighted correlation coefficients and expression levels of these genes, a prognostic model comprising nine CCCR genes was constructed. The formula for the risk score based on the expression of these genes is as follows: Risk Score = (−0.00432685 × C1S expression) + (−0.02426126 × C6 expression) + (−0.06958025 × C7 expression) + (−0.09385343 × F11 expression) + (−0.00169931 × F13B expression) + (−0.00560607 × F7 expression) + (0.069061974 × SERPINE1 expression) + (−0.02283320 × SERPINF2 expression) + (−0.00588306 × SERPING1 expression). The median risk score was used as the cutoff to classify each cohort into high- and low-risk groups.

Kaplan–Meier analysis demonstrated that patients in the high-risk group had significantly lower survival rates than those in the low-risk group in both the training and validation cohorts, with a *P*-value <0.001 (Fig. 2C and **D**). This underscores the effectiveness of the established prognostic model in predicting patient outcomes based on risk scores. To further evaluate the model, distributions of risk scores and survival status were plotted for both cohorts, showing a progressive decline in survival status with increasing risk scores (Fig. 2E–H). Additionally, ROC curve analysis indicated good predictive efficacy of the risk model for 1-, 2-, and 3-year survival rates of patients with HCC, with areas under the ROC curves (AUCs) of 0.714, 0.661, and 0.661, respectively (Fig. 2I). These AUC values were confirmed in the validation group as 0.781, 0.714, and 0.713 at 1, 2, and 3 years, respectively, further validating the predictive capability of the risk model (Fig. 2J). External validation using cohorts GSE14520 and GSE16757 reaffirmed the robustness and reliability of the prognostic value of the CCCR gene signature. Survival analysis in these cohorts (Figs. S2A, C, E and Fig.S2B, D, F, respectively) showed that patients classified as high-risk had worse prognoses compared to those in the low-risk group. The ROC analysis for predicting 1-, 2-, and 3-year overall survival rates yielded AUCs of 0.660, 0.655, and 0.650 for GSE14520 (Fig. S2G) and
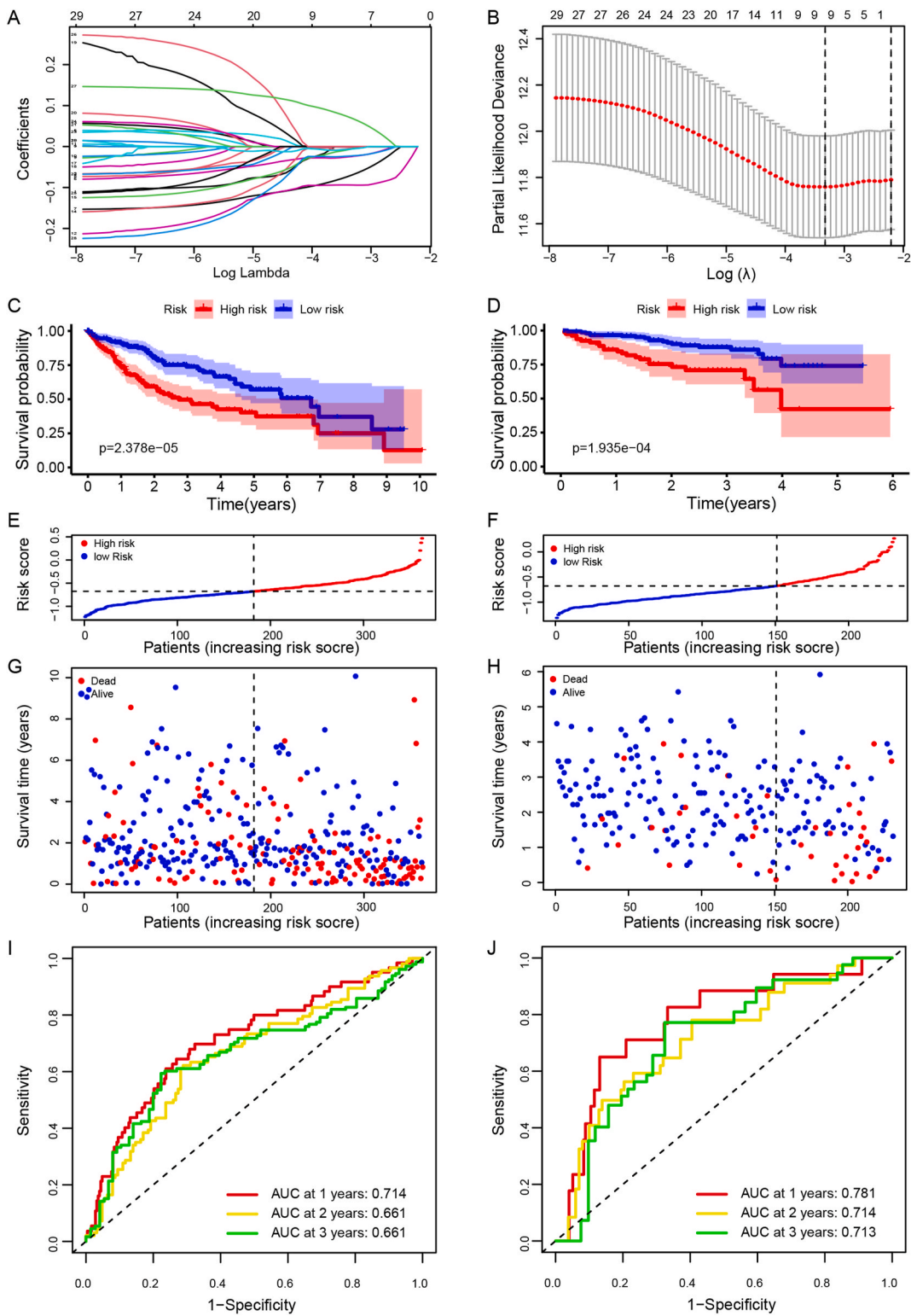
**Fig. 2.** Establishment of a CCCR gene signature in patients with HCC. (A) LASSO coefficient profiles of 29 CCCR genes. (B) Selection of optimal parameter (λ) in the LASSO Cox regression model. (C, D) Kaplan–Meier survival analysis of the prognostic model in the training and validation cohorts. (E, G) Distribution of risk scores and Survival statuses of patients with HCC in the training cohort between high-risk (N = 181) and low-risk (N = 182). (F, H) Distribution of risk scores and Survival statuses of patients with HCC in the validation cohort between high-risk (N = 80) and low-risk (N = 151). (I, J) Area under the curve (AUC) of the prognostic model for predicting 1-, 2-, and 3-year survival rates in the training and validation cohorts.

0.659, 0.660, and 0.662 for GSE16757 (Fig. S2H), further confirming the accurate prognostic value of the high-risk score.

### 3.3. Construction of independent prognostic factors

To investigate the independent predictive effect of the model, univariate and multivariate Cox regression analyses were conducted on both the training and validation cohorts. Variables included sex, age, tumor stage, grade, and risk score. In the training and validation cohorts, stage (HR = 1.504, 95 % CI = 1.211–1.868; HR = 2.395, 95 % CI = 1.207–4.753) and risk score (HR = 3.688, 95 % CI = 1.930–7.050; HR = 3.685, 95 % CI = 1.996–11.352) were identified as significant independent prognostic factors for HCC in both cohorts (Fig. 3A–D). Moreover, tissue grade (HR = 2.192, 95 % CI 1.473–3.261) in the validation cohort was also an independent prognostic factor (Fig. 3C). Interestingly, the hazard ratio of the risk score was notably higher than that of any other clinical parameter.

Furthermore, multivariate ROC curves incorporating risk scores and clinical variables in the training cohort indicated superior effectiveness in predicting HCC survival compared to age, sex, histological grade, or tumor stage alone (Fig. 3E and **F**). Conversely, in the validation cohort, the AUC value for histological grade exceeded that of the risk score, though still below age, sex, and stage (Fig. 3G and **H**). C-index analysis further confirmed the superior prediction accuracy of our risk model (Fig. 3F and **H**). Overall, these findings suggest that our model serves as an independent prognostic factor for determining patient prognosis, with promising clinical applicability.

### 3.4. Constructing predictive nomogram

A nomogram was developed to predict the 1-year, 2-year, and 3-year survival rates of patients with HCC, incorporating independent prognostic factors identified through multivariate Cox regression analysis. Calibration plots were employed to assess the predictive accuracy of the nomograms. The calibration curve closely approximated a diagonal line with a slope of 1, indicating consistent predictions with actual outcomes (Fig. 3I–L). In conclusion, the nomogram, utilizing risk scores and TNM stage, exhibited robust predictive capability for the prognosis of patients with HCC across both training and validation cohorts.

### 3.5. Functional enrichment analyses based on the risk signature

Given the findings from PCA and t-SNE analyses demonstrating the ability of our risk model to effectively distinguish between low- and high-risk groups (Fig. 4A and **B**), we integrated data from the training and validation cohorts to explore distinct functional characteristics. The Wilcoxon test was applied to identify DEGs between these groups within the entire cohort. Using predefined criteria, we identified 996 downregulated and 364 upregulated genes. GO analysis highlighted mitotic nuclear division, mitotic sister chromatid segregation, and chromosome segregation as predominant biological processes in the high-risk group (Fig. 4C). Similarly, KEGG pathway analyses revealed enrichment in the cell cycle, p53 signaling pathway, and cellular senescence (Fig. 4D). Among the downregulated genes, in addition to the complement and coagulation cascades, several metabolism-related pathways such as retinol, amino acid, and fatty acid metabolism were notably involved in the low-risk group (Fig. 4E and **F**).

### 3.6. Differences in immune cell infiltration between high- and low-risk groups

To investigate the infiltration of immune cells and their functions within the tumor microenvironment of high- and low-risk populations, we computed enrichment scores for immune cell subsets using ssGSEA and CIBERSORT algorithms. Within the myeloid cell lineage, ssGSEA analysis revealed a significant reduction in neutrophil infiltration in the high-risk group, although this finding was not corroborated by CIBERSORT analysis (Fig. 5A–D, Fig. S4). Conversely, no significant differences were observed in MDSCs between the high- and low-risk groups (Fig. S3). DC cell infiltration exhibited complex and inconsistent patterns across multiple datasets (Fig. 5A–D, Fig. S4). Notably, macrophage infiltration was increased in the high-risk group in both the training and validation cohorts (P < 0.001). Furthermore, analysis using the CIBERSORT algorithm indicated significant differences in the infiltration of two subsets of macrophages (M0 and M1) between high- and low-risk groups (Fig. 5C and **D**; Fig. S5; Fig. S6).

Within the lymphocyte lineage, B and T helper cells were significantly elevated only in the low-risk group within the training cohort. Additionally, naïve B cells showed higher infiltration in the low-risk group, whereas memory B cells were more prevalent in the high-risk group (Fig. 5C and **D**). Integration of ssGSEA and CIBERSORT algorithms indicated increased Treg infiltration in the high-risk group (Fig. 5A–D; Fig. S4; Fig. S5; Fig. S6).

Analysis of immune functions revealed varied activation or inhibition of multiple immune pathways. Specifically, the type 2 interferon response was significantly downregulated in the high-risk group, whereas MHC class I activation was notably elevated (Fig. 5E and **F**).
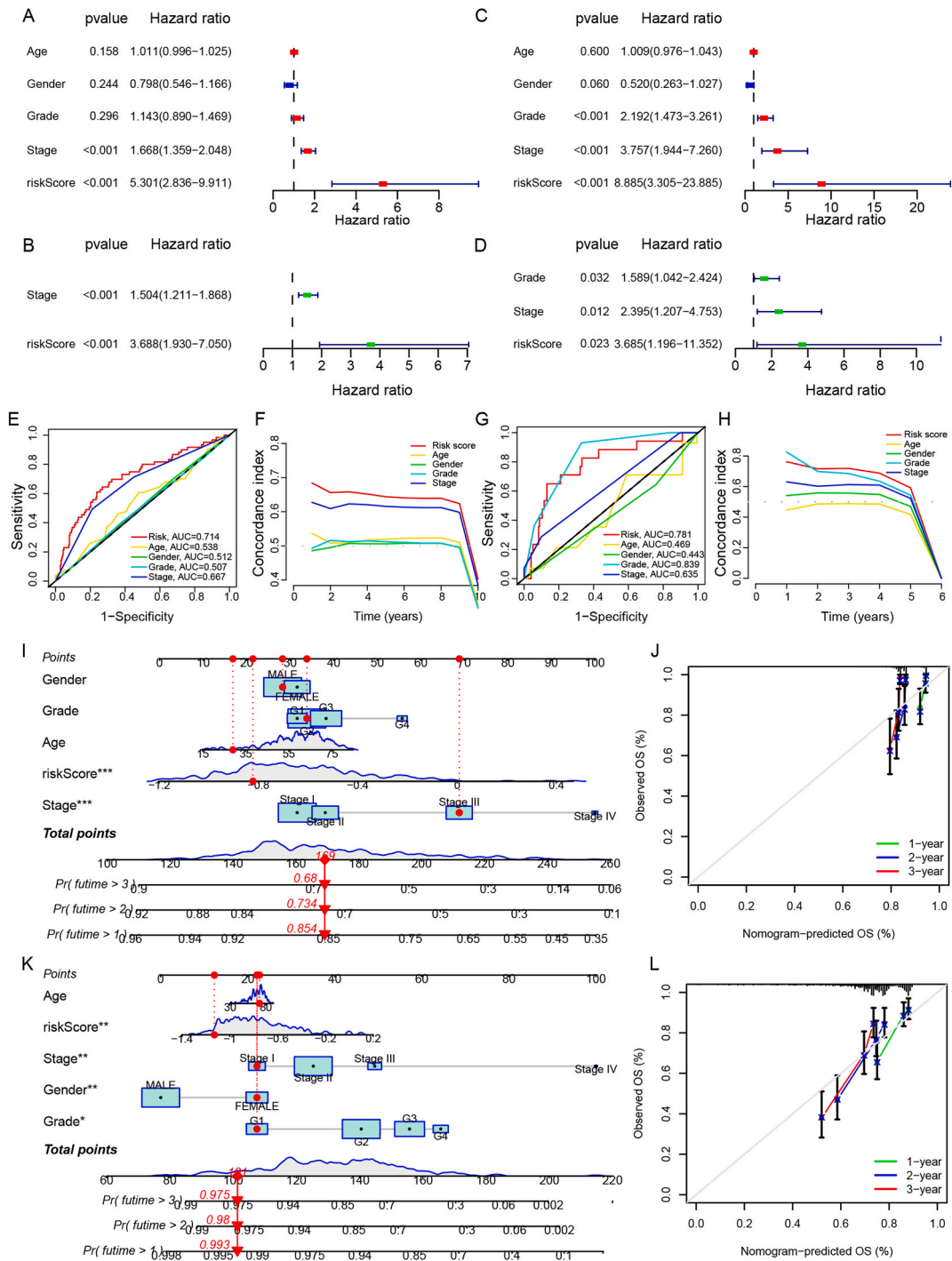
**Fig. 3.** Association between clinicopathological factors and risk score in patients with HCC. (A, B) Forest plot of univariate Cox regression showing associations between RiskScore and clinical factors in the training (A) and validation (B) cohorts. (C, D) Forest plot of multivariate Cox regression illustrating associations between RiskScore and clinical factors in the training (C) and validation (D) cohorts. (E, F) AUC of ROC curves and C-index comparing prognostic accuracy of RiskScore and other factors in the training (E, F) and validation (G, H) cohorts. (I–L) Nomogram and Calibration curve predicting 1-, 2-, and 3-year survival in patients with HCC in the training (I, J) and validation (K, L) cohorts. Statistical significance indicated as * P < 0.05, **P < 0.01, ***P < 0.001, ns for not significant.
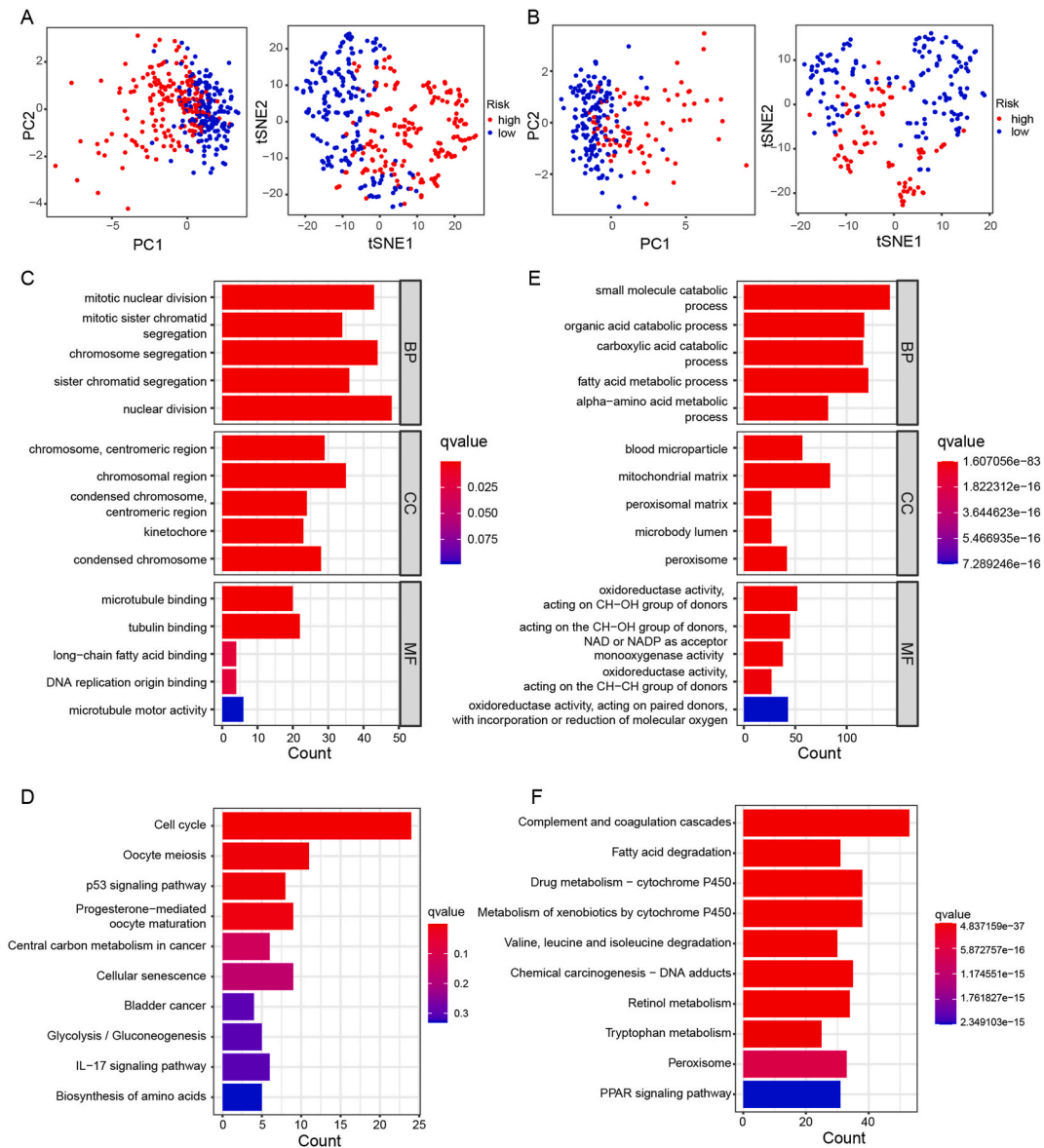
**Fig. 4.** Enrichment analysis in the CCCR genes model. (A) PCA and t-SNE plots comparing high-risk (N = 181) and low-risk (N = 182) group in the training cohorts. (B) PCA and t-SNE plots comparing high-risk (N = 80) and low-risk (N = 151) groups in the validation cohorts. (C, D) Gene Ontology (GO) analysis of differentially expressed genes (DEGs) up-regulated (C) and down-regulated (D) between low- and high-risk groups in the entire cohort. (E, F) KEGG analysis of up-regulated (E) and down-regulated (F) DEGs between low- and high-risk groups in the entire cohort.

### 3.7. Drug sensitivity differential analysis between the two risk groups

To investigate the response to immunotherapy in high- and low-risk groups, we utilized the TIDE algorithm to assess the efficacy of tumor immune checkpoint therapy. TIDE results indicated higher scores in both the training and validation cohorts for the high-risk group, suggesting a reduced likelihood of immune escape in tumor cells and enhanced efficacy of immunotherapy (Fig. 6A and **B**).

Subsequently, we conducted a drug sensitivity analysis between the two risk groups. Leveraging the "OncoPredict" R package and GDSC database, drugs exhibiting statistically significant differences in both cohorts were identified as potential candidates. Our analysis highlighted an elevated IC50 value for JAK1_8709_1718 in the high-risk group (Fig. 6C and **D**). Furthermore, we observed a strong correlation between risk scores and IC50 values (Fig. 6E and **F**). These findings have implications for identifying personalized treatment options for distinct subsets of patients with HCC. Additionally, we explored the relationship between risk scores and drug sensitivity in HCC.
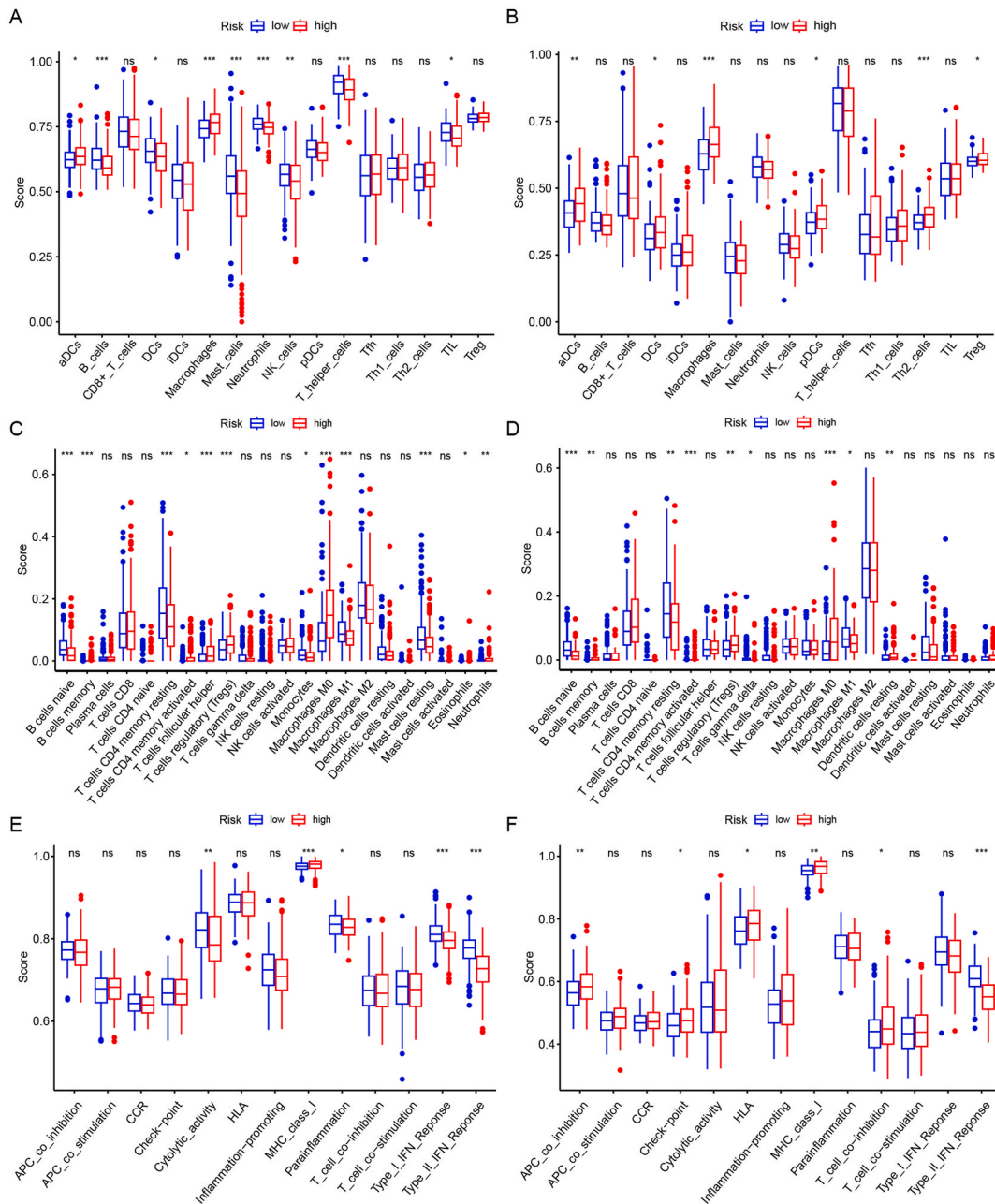
**Fig. 5.** Immune function analysis of CCCR genes signature in the training and validation cohort. (A, B) Comparison of single sample Gene Set Enrichment Analysis (ssGSEA) scores for 16 immune cells between high- and low-risk groups in the training (A) and validation (B) cohorts. (C, D) Boxplots showing proportions of 22 immune cell types based on CIBERSORT in HCC patients between high- and low-risk groups. (E, F) Comparison of ssGSEA scores for 13 immune-related functions between high- and low-risk groups in the training (E) and validation (F) cohorts. P-value calculation is used by wilcox.test. Statistical significance indicated as * P < 0.05, **P < 0.01, ***P < 0.001, ns for not significant.

## 4. Discussion

HCC, characterized by high morbidity and fatality rates, is notable for its pronounced metastatic potential, tumor heterogeneity, and responsiveness to immune-based therapies [1–4]. As the primary producer of complement and coagulation components, the liver environment is significantly influenced by the complement system. Elements of innate immunity and the complement system are present within the tumor microenvironment. The vast array of complement molecules and their multifaceted functions render complement involvement in cancer highly complex and only beginning to be understood [5]. Despite this complexity, no studies have specifically examined the relevance of the CCCR-related pathway in the prognosis and immune microenvironment of HCC. Therefore,
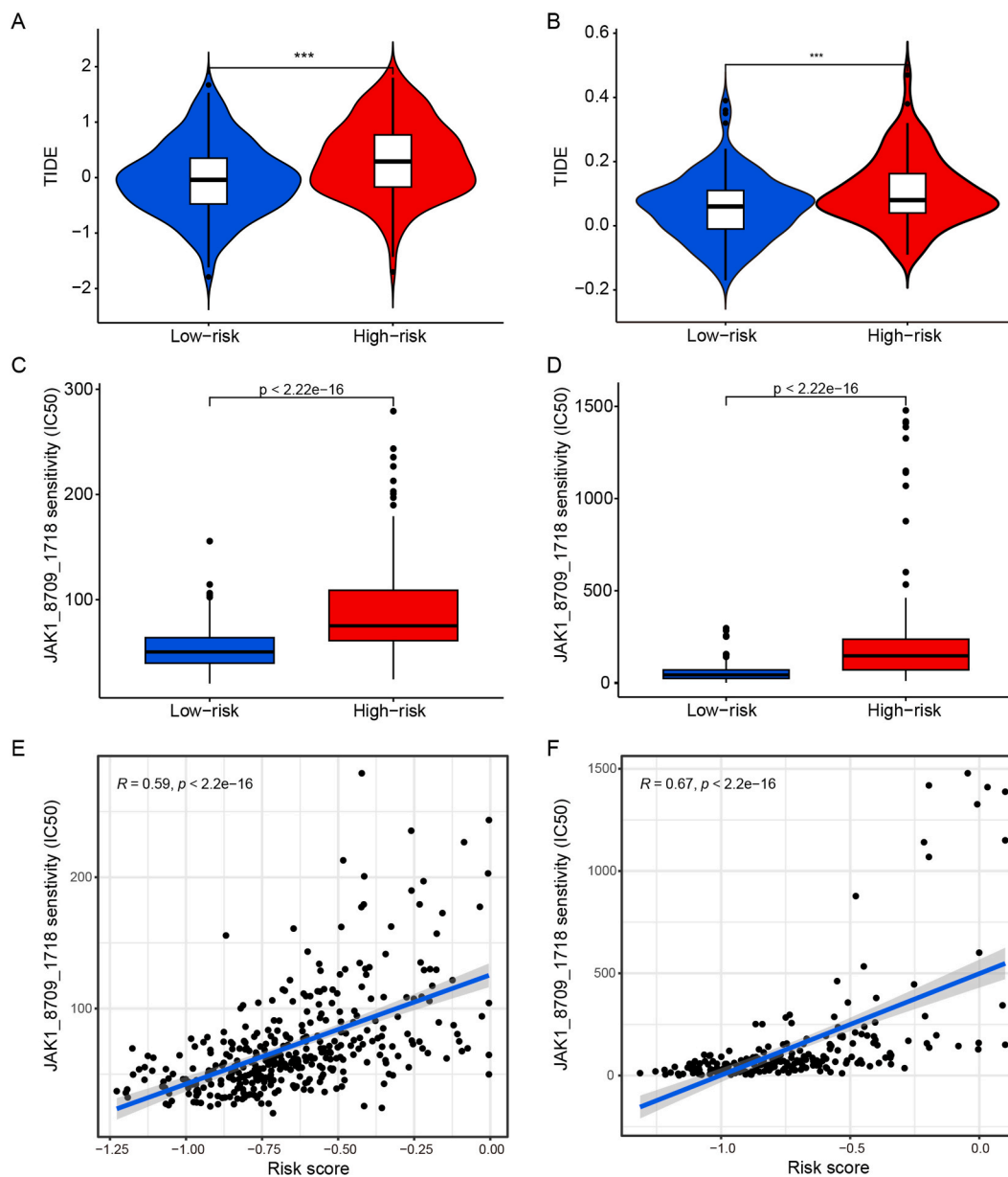
**Fig. 6.** Drug sensitivity analysis of both risk groups. (A, B) Tumor Immune Dysfunction and Exclusion (TIDE) analysis between high- and low-risk groups in the training (A) and validation (B) cohorts, P-value calculation is used by wilcox.test. (C, D) IC50 values of JAK1_8709_1718 sensitivity between high- and low-risk groups in the training (C) and validation (D) cohorts, P-value calculation is used by wilcox.test. (E, F) Correlation between IC50 values of JAK1_8709_1718 and Risk score in the training (E) and validation (F) cohorts was calculated by spearman correlation analysis. Statistical significance indicated as ***P < 0.001.

our objective was to elucidate the impact of the complement and coagulation systems on prognosis, changes in the immune microenvironment, tumor immune evasion, and therapeutic response in HCC.

In this study, we selected nine signature genes, including both upregulated (F13B) and downregulated genes (C1S, C6, C7, F7, F11, SERPINE1, SERPINE2, and SERPING1), to establish a risk model capable of accurately assessing the prognosis of patients with HCC. By stratifying patients based on their CCCR gene expression profiles, our model provides a robust tool for prognostication, aiding clinicians in identifying high-risk patients who may benefit from more intensive monitoring and treatment. Complement-related genes such as C6 and C7 have demonstrated prognostic significance in HCC, consistent with previous findings [17]. SERPING1, encoding a C1 inhibitor protein critical for complement regulation by inhibiting C1s and C1r activation, however, its prognostic impact in HCC remains uncertain.

We also investigated the prognostic relevance of coagulation cascade-related genes in HCC. Most of these genes were

downregulated in patients with HCC, possibly due to disease progression impairing liver synthesis. However, the expression of F13B was elevated in patients with HCC, consistent with previous proteomic research [9]. One possible explanation is that elevated F13B levels in patients with HCC may correlate with increased bloodstream metastases, potentially leading to a poorer prognosis. In contrast to F13B, both F7 and F11 were significantly downregulated in patients with HCC. F7, encoding coagulation factor VII, is associated with hepatic metastasis in colorectal cancer through tissue factor binding [18]. Du et al. demonstrated that the lncRNA F11 Antisense RNA 1 is underexpressed in HCC, supporting our findings [19]. Additionally, SERPINE1 and SERPINE2, members of the serpin family, are downregulated in patients with HCC. While upregulation of SERPINE1 promotes cancer cell invasion and migration via the PI3K-Akt pathway, studies suggest that its downregulation significantly impacts survival rates in both HCC and normal individuals [20, 21]. SERPINE2 is implicated in inflammation-mediated malignancy and vascular normalization disruption [22].

However, the relationship between CCCR genes and immune cell infiltration in HCC remains unclear. Our study revealed that the high-risk group exhibited elevated scores for immune cell infiltration, including M0 macrophages, activated memory CD4 T cells, memory B cells, and Tregs. In contrast, macrophage M1, resting memory CD4$^+$ T cells, and naive B cells had higher scores in the low-risk group. Furthermore, we observed significant positive correlations between macrophages and Tregs with the CCCR risk score. Notably, macrophages (M0 and M1) differed significantly between the high- and low-risk groups, whereas M2 macrophages showed no significant difference between the groups. Previous studies have underscored the adverse prognostic role of M0 macrophages not only in HCC but also in gastric and endometrial cancers [23,24]. Conversely, the anti-tumor effect of M1 macrophages constitutes a crucial component of the Th1 immune response initiated by antigen presentation mechanisms [25]. In early cancer stages, increased secretion of pro-inflammatory factors by M1 macrophages attracts and activates T cells, thereby initiating an immune response against cancer cells that may lead to their elimination [26]. Therefore, we speculate that differences between M0 and M1 macrophages may hold significant research value in HCC pathogenesis.

Previous research has indicated that increased infiltration of T regulatory cells (Tregs) correlates with poor prognosis in patients with HCC [27,28]. Consistent with our initial findings, we observed significantly higher Treg cell infiltration in high-risk groups across four independent cohorts. Immune function analysis results showed upregulation of MHC class I in the high-risk group, potentially shielding tumor cells from macrophage phagocytosis, while type II IFN response was decreased, possibly impacting cancer immunosurveillance [29]. Collectively, targeting CCCR pathways involved in macrophage regulation could potentially tilt the balance towards a more immunostimulatory TME. Additionally, strategies such as vaccine-induced immune stimulation or adoptive Treg cell therapies may prove beneficial. This approach, combined with other immunotherapies, holds promise for enhancing immune responses and offering treatment options for high-risk patients with HCC.

In this study, our model revealed that the high-risk group exhibited significant potential for immune evasion, whereas low-risk patients showed a propensity to benefit from immune-based treatments. Additionally, we identified a promising candidate, JAK1 inhibitor (JAK1_8709_1718), suitable for low-risk patients. Ruxolitinib, a selective JAK1/2 inhibitor, has been shown to impede liver fibrosis and slow HCC progression [30]. The JAK-STAT pathway has emerged as a promising target for HCC treatment [31,32], with JAK1_8709_1718 standing out as a novel, potent, and specific therapeutic agent for HCC. Targeting this pathway may enhance the efficacy of antitumor therapies and introduce a novel treatment avenue for patients with HCC.

Nevertheless, our study has several limitations. Primarily, the results relied on public databases and bioinformatics analyses, lacking experimental validation. Future studies should further validate the prognostic model across diverse patient populations and clinical settings, addressing challenges such as data privacy, security, and the establishment of standardized guidelines and decision-support tools. Due to limited ICI data availability, we were unable to comprehensively analyze the predictive role of the CCCR risk score for ICIs. Moreover, the biological and medical mechanisms underlying CCCR genes in HCC progression warrant deeper exploration in future research.

In summary, we developed a prognostic model based on CCCR genes to assess the potential of immunotherapy and explore its correlation with drug sensitivity in HCC. This model serves as a robust tool for predicting survival, guiding treatment decisions, and stratifying patients with HCC who may benefit from anticancer immunotherapy. Thus, our findings gained from implementing this model can inform future research on the role of CCCR genes in HCC and other cancers, contributing to the development of novel therapeutic strategies.

**Ethics approval and consent to participate**

The study protocol was approved by The Ethics Committee of Ningbo No. 2 Hospital (Zhejiang, China) and was conducted according to the principles of the Declaration of Helsinki.

**Consent for publication**

Not applicable.

**Availability of data and materials**

Raw data were downloaded from databases such as the University of California Santa Cruz Xena browser (UCSC Xena, http://xena.ucsc.edu), the International Cancer Genomics Consortium (ICGC, dcc.icgc.org) and the GEO database without any restrictions. The authors have made the raw data supporting the conclusion of this article available to all qualified researchers without undue reservation.

## Funding information

## CRediT authorship contribution statement

**Hui Su:** Data curation. **Yunjie Chen:** Writing – original draft. **Wuke Wang:** Funding acquisition, Formal analysis.

## Declaration of competing interest

The authors declare that they have no known competing financial interests or personal relationships that could have appeared to influence the work reported in this paper.

## Acknowledgements

## Appendix A. Supplementary data

Supplementary data to this article can be found online at https://doi.org/10.1016/j.heliyon.2024.e38230.

## References

[1] H. Sung, et al., Global cancer statistics 2020: GLOBOCAN estimates of incidence and mortality worldwide for 36 cancers in 185 countries, CA Cancer J Clin 71 (3) (2021) 209–249.

[2] A. Forner, M. Reig, J. Bruix, Hepatocellular carcinoma, Lancet 391 (10127) (2018) 1301–1314.

[3] G.P. Dunn, C.M. Koebel, R.D. Schreiber, Interferons, immunity and cancer immunoediting, Nat. Rev. Immunol. 6 (11) (2006) 836–848.

[4] B. Sangro, et al., Advances in immunotherapy for hepatocellular carcinoma, Nat. Rev. Gastroenterol. Hepatol. 18 (8) (2021) 525–543.

[5] E.B. Thorgersen, et al., The role of complement in liver injury, regeneration, and transplantation, Hepatology 70 (2) (2019) 725–736.

[6] A. Walakira, et al., Integrative computational modeling to unravel novel potential biomarkers in hepatocellular carcinoma, Comput. Biol. Med. 159 (2023) 106957.

[7] J. Yao, et al., Profiling, clinicopathological correlation and functional validation of specific long non-coding RNAs for hepatocellular carcinoma, Mol. Cancer 16 (1) (2017) 164.

[8] Y. Yuan, et al., Ficolin 3 promotes ferroptosis in HCC by downregulating IR/SREBP axis-mediated MUFA synthesis, J. Exp. Clin. Cancer Res. 43 (1) (2024) 133.

[9] Y. Zhang, et al., C8B in complement and coagulation cascades signaling pathway is a predictor for survival in HBV-related hepatocellular carcinoma patients, Cancer Manag. Res. 13 (2021) 3503–3515.

[10] W. Dong, et al., Proteomic analysis of small extracellular vesicles from the plasma of patients with hepatocellular carcinoma, World J. Surg. Oncol. 20 (1) (2022) 387.

[11] W. Zhang, Critical roles of S100A12, MMP9, and PRTN3 in sepsis diagnosis: insights from multiple microarray data analyses, Comput. Biol. Med. 171 (2024) 108222.

[12] Y. Zhang, et al., A signature for pan-cancer prognosis based on neutrophil extracellular traps, J Immunother Cancer 10 (6) (2022).

[13] Y. Fu, et al., Genome-wide identification of FHL1 as a powerful prognostic candidate and potential therapeutic target in acute myeloid leukaemia, EBioMedicine 52 (2020) 102664.

[14] T. Le, et al., A review of digital cytometry methods: estimating the relative abundance of cell types in a bulk of cells, Briefings Bioinf. 22 (4) (2021).

[15] Y. Qin, et al., Cuproptosis correlates with immunosuppressive tumor microenvironment based on pan-cancer multiomics and single-cell sequencing analysis, Mol. Cancer 22 (1) (2023) 59.

[16] M. Pak, et al., Improved drug response prediction by drug target data integration via network-based profiling, Briefings Bioinf. 24 (2) (2023).

[17] X. Qian, et al., The role of complement in the clinical course of hepatocellular carcinoma, Immun Inflamm Dis 10 (3) (2022) e569.

[18] Y.W. van den Berg, et al., The relationship between tissue factor and cancer progression: insights from bench and bedside, Blood 119 (4) (2012) 924–932.

[19] J. Du, et al., LncRNA F11-AS1 suppresses liver hepatocellular carcinoma progression by competitively binding with miR-3146 to regulate PTEN expression, J. Cell. Biochem. 120 (10) (2019) 18457–18464.

[20] Y. Lu, et al., Traditional Chinese medicine syndromes classification associates with tumor cell and microenvironment heterogeneity in colorectal cancer: a single cell RNA sequencing analysis, Chin. Med. 16 (1) (2021) 133.

[21] G. Zhang, et al., Dissecting a hypoxia-related angiogenic gene signature for predicting prognosis and immune status in hepatocellular carcinoma, Front. Oncol. 12 (2022) 978050.

[22] J. Hou, et al., YTHDF2 reduction fuels inflammation and vascular abnormalization in hepatocellular carcinoma, Mol. Cancer 18 (1) (2019) 163.

[23] J. Long, et al., Development and validation of a TP53-associated immune prognostic model for hepatocellular carcinoma, EBioMedicine 42 (2019) 363–374.

[24] B. Tang, et al., Diagnosis and prognosis models for hepatocellular carcinoma patient's management based on tumor mutation burden, J. Adv. Res. 33 (2021) 153–165.

[25] J.A. You, et al., WGCNA, LASSO and SVM algorithm revealed RAC1 correlated M0 macrophage and the risk score to predict the survival of hepatocellular carcinoma patients, Front. Genet. 12 (2021) 730920.

[26] K. Vinnakota, et al., M2-like macrophages induce colon cancer cell invasion via matrix metalloproteinases, J. Cell. Physiol. 232 (12) (2017) 3468–3480.

[27] Y.H. Lee, et al., IFNgamma(-)IL-17(+) CD8 T cells contribute to immunosuppression and tumor progression in human hepatocellular carcinoma, Cancer Lett. 552 (2023) 215977.

[28] C.J. Lim, et al., Multidimensional analyses reveal distinct immune microenvironment in hepatitis B virus-related hepatocellular carcinoma, Gut 68 (5) (2019) 916–927.

[29] A.A. Barkal, et al., Engagement of MHC class I by the inhibitory receptor LILRB1 suppresses macrophages and is a target of cancer immunotherapy, Nat. Immunol. 19 (1) (2018) 76–84.

[30] Z. Song, et al., Ruxolitinib suppresses liver fibrosis progression and accelerates fibrosis reversal via selectively targeting Janus kinase 1/2, J. Transl. Med. 20 (1) (2022) 157.

[31] R. Peng, et al., Down-regulation of circPTTG1IP induces hepatocellular carcinoma development via miR-16-5p/RNF125/JAK1 axis, Cancer Lett. 543 (2022) 215778.

[32] L. Yang, et al., CircularRNA-9119 protects hepatocellular carcinoma cells from apoptosis by intercepting miR-26a/JAK1/STAT3 signaling, Cell Death Dis. 11 (7) (2020) 605.